A Registration-Based Approach to Quantify Flow-Mediated Dilation (FMD) of the Brachial Artery in Ultrasound Image Sequences

Alejandro F. Frangi*, *Associate Member, IEEE*, Martín Laclaustra, and Pablo Lamata

***Abstract*—Flow-mediated dilation (FMD) offers a mechanism to characterize endothelial function and, therefore, may play a role in the diagnosis of cardiovascular diseases. Computerized analysis techniques are very desirable to give accuracy and objectivity to the measurements. Virtually all methods proposed up to now to measure FMD rely on accurate edge detection of the arterial wall, and they are not always robust in the presence of poor image quality or image artifacts. A novel method for automatic dilation assessment based on a global image analysis strategy is presented. We model interframe arterial dilation as a superposition of a rigid motion and a scaling factor perpendicular to the artery. Rigid motion can be interpreted as a global compensation for patient and probe movements, an aspect that has not been sufficiently studied before. The scaling factor explains arterial dilation. The ultrasound sequence is analyzed in two phases using image registration to recover both transformation models. Temporal continuity in the registration parameters along the sequence is enforced with a Kalman filter since the dilation process is known to be a gradual physiological phenomenon. Comparing automated and gold standard measurements (average of manual measurements) we found a negligible bias (0.05%FMD) and a small standard deviation (SD) of the differences (1.05%FMD). These values are comparable with those obtained from manual measurements ($\text{bias} = 0.23\%\text{FMD}$, $\text{SD}_{\text{intra-obs}} = 1.13\%\text{FMD}$, $\text{SD}_{\text{inter-obs}} = 1.20\%\text{FMD}$). The proposed method offers also better reproducibility ($\text{CV} = 0.40\%$) than the manual measurements ($\text{CV} = 1.04\%$).**

***Index Terms*—Endothelial function, flow-mediated dilation, image registration, ultrasound.**

I. Introduction

ASSESSMENT and characterization of endothelial function in the diagnosis of cardiovascular diseases is a current clinical research topic [1], [2]. The endothelium shows measurable responses to flow changes [3], [4], and flow-mediated dilation (FMD) may, therefore, be used for assessing endothelial health; B-mode ultrasonography (US) is a cheap and noninvasive way to estimate this dilation response [5]. However, complementary computerized image analysis techniques are still very desirable to give accuracy and objectivity to the measurements [1].

Several methods based on the detection of edges of the arterial wall have been proposed over the last ten years. The first studies used a tedious manual procedure [5], which had a high interobserver variability [6]. Some interactive methods tried to reduce this variability by attracting manually drawn contours to image features, like the maximum image gradient, where the vessel wall is assumed to be located [7]–[10]. Some more recent efforts are focused on dynamic programming or deformable models [11]–[18], and on neural networks [19].

All these methods present some common limitations. First, edge detection techniques are undermined by important error sources like speckle noise or the varying image quality typical of US sequences. Second, most methods require expert intervention to manually guide or correct the measurements, thus being prone to introduce operator-dependent variability. Also, almost no method performs motion compensation to correct for patient and probe position changes. This could easily lead to measuring arterial dilation using wrong anatomical correspondences. Temporal continuity is another aspect that has not been exploited enough in previous work. Two consecutive frames have a high correlation, and only Newey *et al.* [19] and Fan *et al.* [15] take advantage of this feature during edge detection. Finally, there is a general lack of large-scale validation studies in most of the techniques presented so far.

In this paper, a method is proposed which is based on a global strategy to quantify flow-mediated vasodilation. We model interframe arterial vasodilation as a superposition of a rigid motion (translation and rotation) and a scaling factor normal to the artery. Rigid motion can be interpreted as a global compensation for patient and probe movements. The scaling factor explains arterial vasodilation. The US sequence is analyzed in two phases using image registration to recover both rigid motion and vasodilation. Image registration uses normalized mutual information (NMI) [20] and a multiresolution framework [21]. Temporal continuity of registration parameters along the sequence is enforced with a Kalman filter [22]. Application of constraints on the vasodilation dynamics is a natural step, since the dilation process is known to be a gradual and continuous physiological phenomenon.

The paper is organized as follows. Section II describes the system for image acquisition and the protocol for a typical FMD study. It also describes the population used to evaluate

Manuscript received January 31, 2003; revised July 24, 2003. This work was supported in part by the Spanish Ministry of Science and Technology under Grant TIC2002-04495-C02. The work of A. F. Frangi was supported by the Spanish Ministry of Science and Technology under a Ramón y Cajal Research Fellowship. *Asterisk indicates corresponding author.*

*A. F. Frangi is with the Division of Biomedical Engineering, Aragon Institute of Engineering Research, Universidad de Zaragoza, María de Luna, 1. Ada Byron Building. Room D.2.03, E-50018 Zaragoza. Spain (e-mail: afrangi@unizar.es).

M. Laclaustra is with the Hospital Clínico Lozano Blesa, Aragon Institute of Health Sciences, E-50009 Zaragoza, Spain.

P. Lamata is with the Computer Vision Group, Division of Biomedical Engineering, Aragon Institute of Engineering Research, University of Zaragoza, E-50018 Zaragoza, Spain.

Digital Object Identifier 10.1109/TMI.2003.819278

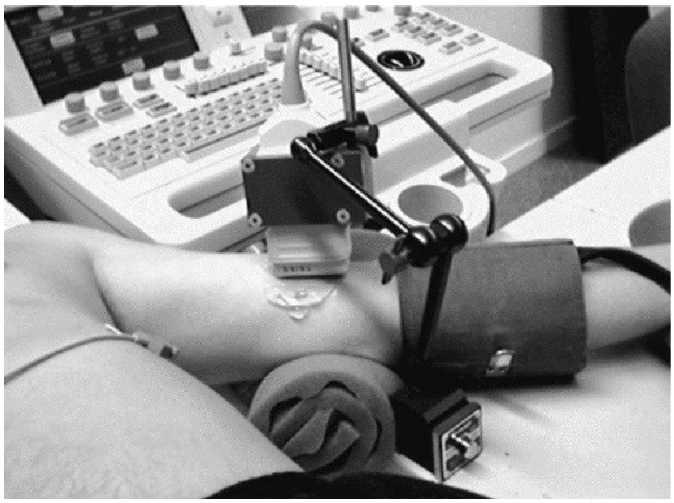

Fig. 1. Experimental setup.

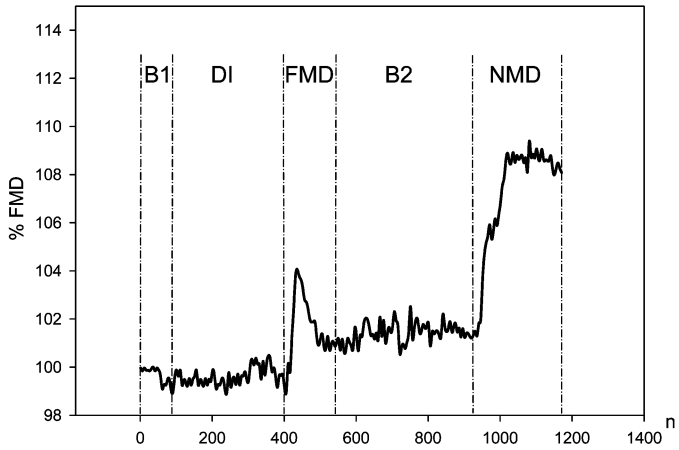

Fig. 2. A whole typical examination is made up of several segments along the sequence: B1, DI, FMD, B2, and NMD.

our technique. Section III introduces the proposed method to assess FMD. The validation of the technique is reported in Section IV. In Section V, the results are discussed and some concluding remarks are made in Section VI.

II. Materials

A. Subjects

A total of 195 sequences of varying image quality were studied, corresponding to 195 male volunteers of the Spanish Army (age range, 34–36 years). This sample is part of the AGEMZA Study, a national cohort study of cardiovascular risk factors in young adults and includes subjects with a wide range of clinical characteristics (body weight: 62.3 –111.8 Kg; body mass index: 20.59 –35.36 $\mathrm{Kg/m^2}$; hypertension: 9%; hypercholesterolemia: 20%; smokers: 24%).

B. Image Acquisition

Image acquisition was carried out at the Hospital Clínico Universitario Lozano Blesa (Zaragoza, Spain). The echographic probe was positioned onto the arm of the patient lying supine on a bed. A silicon gel was used as impedance adapter for better ultrasound wave transmission. The probe, once the correct orientation angle was found, was fixed with a probe holder to the table where the patient's arm lies (Fig. 1). Telediastolic images were captured and hold, coincident with the peak of the R wave of the electrocardiogram. A SONOS 4500 (Agilent Technologies, Andover, MA) ultrasound system was used in frequency fusion mode and employing a 5–7.5 MHz trapezoidal multifrequency probe. Images were transferred to a frame grabber via a video Y/C link and images were digitized at a resolution of 768×576 pixels.

During the examination, unavoidable movements take place, thus changing the relative position between the transducer and the artery. Therefore, expert intervention is sometimes required to control the image quality by readjusting the orientation of the transducer to keep visible borders as sharp as possible. Both, motion artifacts and successive readjustments may induce changes in image quality as well as changes on extra-luminal structures along the sequence. All these factors have to be handled appropriately in the postprocessing stage if the computerized analysis has to be used on a routine basis.

Each sequence has about 1200 frames and a duration of around 20 min, acquiring each second the last telediastolic frame previously hold. This provides a fixed sampling rate irrespective of heart rate, which means a substantial benefit for clinical interpretation, as different stimulus are applied on a time basis along the clinical test. As the dynamics of endothelial vasodilation is much slower than changes happening between cardiac cycles, with this sampling rate, missing information from one heartbeat or using one heartbeat twice does not affect, in practice, the results.

FMD is the vasodilation response to hyperemia after a transitory distal ischemia (DI) induced in the forearm using a pneumatic cuff distal to the probe (Fig. 1). The dilation mediated by a chemical vasodilator, the nitroglycerine, or nitroglycerine-mediated dilation (NMD), is also registered. Accordingly, five phases of the medical test can be distinguished in each sequence (see Fig. 2).

- **Rest baseline (B1)**. Initial rest state preceding DI. Presents the best image quality in the whole sequence and lasts for about 1 min.
- **Distal ischemia (DI)**. The cuff is inflated and, therefore, the image quality is usually the worst in the sequence. It takes approximately 5 min. This phase ends when the cuff pressure is released.
- **Flow-mediated dilation (FMD)**. Response to reactive hyperemia. The maximum %FMD of healthy subjects has a mean value around 5%, and it takes place about 60 s after the cuff is released [5]. At the beginning of this phase, and coincident with the release of the cuff, it is common to have important motion artifacts. The duration of this phase depends on each patient.
- **Post-FMD baseline (B2)**. The artery diameter returns to a steady state. This state does not necessary have to coincide with that of B1.
- **Nitroglycerine-mediated dilation (NMD)**. Response to the sublingual supply of a fixed dose of this chemical vasodilator, which is made 8 min later than the cuff release.

Fig. 3. Overview of the proposed two-stage method: after motion compensation is carried out by recovering a rigid motion model, the vasodilation is measured by computing the scaling factor along the normal to the artery that best matches the two analyzed frames.

III. Proposed Method

A. Algorithm Overview

Our technique assumes that the vasodilation that takes place between two frames can be modeled by a constant scaling in the direction normal to the artery. This scale factor is obtained by means of image registration.

A reference frame is selected from the beginning of the sequence. All the other frames are registered to this reference frame. Changes in the relative position between the patient and the transducer are quite common during a whole examination, which may take up to 20 min. To elude wrong anatomical correspondences, motion compensation becomes necessary, and a rigid image registration technique is used to this end.

Structures surrounding the artery in the image may be important to resolve potential ambiguities in the longitudinal alignment between two frames, which occur because of the lineal nature of the arterial walls. On the other hand, extra-luminal structures introduce artifacts when measuring the vasodilation since they do not necessarily deform in the same way as the artery does. Therefore, they should be taken into account when retrieving the global rigid motion information of the model, whilst arterial vasodilation estimation should only consider the artery deformation.

Our technique proceeds in two phases as summarized in Fig. 3: motion compensation and dilation assessment. The first phase uses the original frames and rigid image registration to recover a rigid motion model. Translation and rotation parameters are used to initialize the subsequent phase of vasodilation estimation. This second stage employs an affine registration model. To avoid artifacts when measuring arterial vasodilation it is convenient to remove background extra luminal structures by padding them out from the reference frame. Preprocessing of this frame also requires repositioning it so that the artery is normal to the scaling direction, that is to say, aligned with the horizontal axis, since our model searches for a vertical scaling factor (see Fig. 4). Both operations are performed manually on the reference frame. Manual masking only requires to roughly draw two lines in the reference frame and repositioning, to align a line with the direction of the artery, a process that is simple and takes only a few seconds per image sequence.

Temporal continuity is enforced in both phases by means of a Kalman filter in the registration parameter space prior to registering each new frame.

In the next two subsections the registration algorithm and its initialization, enforcing temporal continuity, are discussed.

B. Registration Algorithm

1) Motion and Vasodilation Models: Registering image B onto image A requires finding a transformation $T(\cdot)$ that maps B into A by maximizing a registration measure $M(\cdot)$ as indicated in (1). The similarity measure is computed over all points, P, of the overlap region of both images

$$M(A(P), B(T(P))). \tag{1}$$

Our motion model between the original (x, y) and transformed (x', y') coordinates is a rigid transformation of the form

$$\begin{pmatrix} x' \\ y' \end{pmatrix} = \begin{pmatrix} \cos\theta & -\sin\theta \\ \sin\theta & \cos\theta \end{pmatrix} \cdot \begin{pmatrix} x \\ y \end{pmatrix} + \begin{pmatrix} t_x \\ t_y \end{pmatrix}. \tag{2}$$

As we are imaging only a small and roughly straight vessel segment, the vasodilation can be assumed to be normal to the artery and, therefore, it can be modeled by only a scaling factor in that direction. Then, the vasodilation model is a similarity transformation with four degrees of freedom (DOFs)

$$\begin{pmatrix} x' \\ y' \end{pmatrix} = \begin{pmatrix} \cos\theta & -S_y \cdot \sin\theta \\ \sin\theta & S_y \cdot \cos\theta \end{pmatrix} \cdot \begin{pmatrix} x \\ y \end{pmatrix} + \begin{pmatrix} t_x \\ t_y \end{pmatrix}. \tag{3}$$

2) Registration Measure: Several registration measures have been traditionally used in medical image matching and they main ones are listed in Table I.

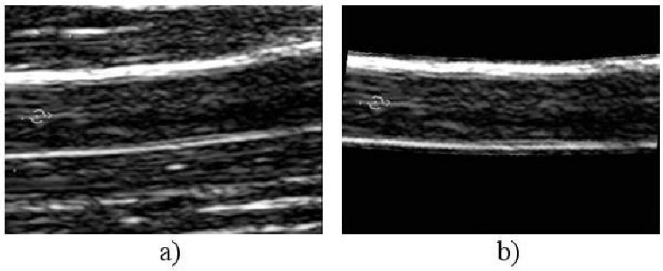

Fig. 4. Preprocessing applied to the reference frame before the phase of vasodilation assessment. a) Original reference frame, and b) the reference frame after alignment to the horizontal axis and padding out of background structures.

TABLE I
Different Similarity Measures

SSD	Sum of Squared Differences
CC	Cross Correlation
GCC	Gradient image Cross Correlation
JE	Joint Entropy
MI	Mutual Information
NMI	Normalized Mutual Information

Among the different similarity measures, NMI is selected in this work owing to its low sensitivity to the size of the overlap region [20], and due to its higher accuracy (See Section IV-B2. This measure, is defined as

$$\mathrm{NMI}(A, B) = \frac{H(A) + H(B)}{H(A, B)} \tag{4}$$

where $H(A)$ is the entropy of image A defined as

$$H(A) = -\sum_i p_i \cdot \log p_i \tag{5}$$

and $H(A, B)$ is the joint entropy between images A and B defined as

$$H(A, B) = -\sum_{i,j} p_{i,j} \ \log \ p_{i,j}. \tag{6}$$

The entropies are computed from the image histograms where p_i is an approximation of the probability of occurrence of inten-

TABLE II
SUMMARY OF REGISTRATION PARAMETERS

Parameter	Symbol	Value
Registration measure	M	See Table I
No. of bins in joint histogram discretization	b	64
Gaussian kernel width for pre-blurring	σ_b	1
Resampling ratio	ρ	1.5
No. of resolution levels	r	3
Interpolation scheme	-	Bilinear

sity value i. Similarly, the joint entropy is computed from the joint histogram where $p_{i,j}$ is the approximation of the probability of the occurrence of corresponding intensity pairs (i, j). Linear interpolation is used to obtain intensities in noninteger pixel values to build the joint histograms.

3) Optimization Algorithm: A multiresolution framework proposed by Studholme *et al.* [21] is employed to recover the optimal transformation. The image is iteratively sub-sampled by a factor of two to build a multiresolution image pyramid. The registration problem is solved at each pyramid level in a coarse to fine fashion. The registration parameters found at each level are used as starting estimates for the parameters at the next level.

4) Summary of Registration Parameters: In Table II, a summary of the parameters of the registration algorithm is provided. To compute the several registration metrics of Table I, the joint histogram is discretized using 64×64 bins. Prior to image registration, the images are prefiltered with a Gaussian kernel of $\sigma_b = 1$ pixel and the images are resampled to a new pixel-size of 1.5 with respect to the original size. These two steps can help to reduce small-scale noise and to reduce the computational load, and yield seemly registration results. Finally, the optimization strategy proceeds in three resolution levels. Image interpolation is carried out using a bilinear interpolation scheme.

C. Temporal Continuity

In order to perform motion compensation and vasodilation assessment, it is convenient to introduce prior knowledge about the smooth nature of the arterial vasodilation process. This *a priori* information could be used to filter out sharp transitions in the vasodilation parameter, which arise as a consequence of registration errors and which are not physiologically plausible. Moreover, these registration errors could easily propagate to the following frames, thus invalidating all subsequent measurements.

To avoid error propagation and impose constraints on the vasodilation dynamics, a Kalman filter [22] is employed in order to improve the estimation of the initial registration parameters. This filter recursively weights each new measurement vector, $\mathbf{Y}(n)$, with the accumulated history to elaborate the next estimate of a state vector, $\mathbf{X}(n)$, which describes the internal behavior of a system. According to this technique a state vector is estimated, $\tilde{\mathbf{X}}(n)$, from an observation or measurement vector $\mathbf{Y}(n)$ and an *a priori* prediction of the state, $\hat{\mathbf{X}}(n)$, made only on the basis of state history. A state and an observation model are employed. The state is modeled as a Gaussian process $\mathbf{v}_1(n)$ with power $\mathbf{Q}_1(n)$, and a transition matrix $\mathbf{F}(n, n-1)$ used to make the predictions. The observation model is known with an uncertainty also modeled by a Gaussian process $\mathbf{v}_2(n)$ with power $\mathbf{Q}_2(n)$, and an observation matrix $\mathbf{C}(n)$ that relates state and observation vectors (see Fig. 5). The Kalman gain $\mathbf{G}_k(n)$ weights new information (innovation) provided by current observations. The estimation is made according to

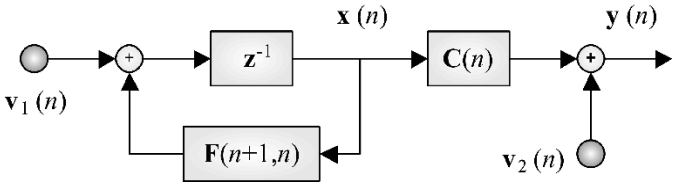

Fig. 5. Kalman filter state and observation models.

$$\tilde{\mathbf{X}}(n) = \hat{\mathbf{X}}(n) + \mathbf{G_k}(n) \times (\mathbf{Y}(n) - \mathbf{C}(n) \times \hat{\mathbf{X}}(n)). \quad (7)$$

In our case, the state vector $\mathbf{X}(n)$ accounts for the position, rotation and scaling of the artery in each frame with respect to the reference frame; the measurement vector, $\mathbf{Y}(n)$, registers the parameters output by the registration algorithm. Therefore, $\mathbf{C}(n)$ equals the identity matrix as in our problem the states are directly observable.

In the next two subsections, the elaboration of the starting estimates in the motion compensation and in the vasodilation stages are presented.

1) Starting Estimate in Motion Compensation: The state vector in the motion compensation phase involves three components: two translation parameters, t_x and t_y, and a rotation angle, θ. It has not been possible to derive an elaborated linear model of the dynamics of these parameters owing to the strong nonstationary behavior of the motion artifacts. Without this model it becomes very difficult to estimate $Q_1(n)$ and $Q_2(n)$.

In this situation, we used a motion model using a zero-order prediction scheme where $\mathbf{F}(n, n-1)$ is the identity matrix indicating that the next state equals the current state and, therefore, a constant Kalman gain, G_k is used. In this way, a systematic inertia is introduced during motion tracking that minimizes falling into wrong local minima not temporally consistent with previous history of arterial motion; on the other hand, it might also slow down the ability to track sudden transitions coming from true motion artifacts. A Kalman gain of 0.1 has empirically shown to be a good compromise between these two competing goals and it was used throughout our experiments.

2) Starting Estimate During Vasodilation Assessment: In this stage, we assume that the translation and rotation parameters were correctly recovered at the motion compensation stage.

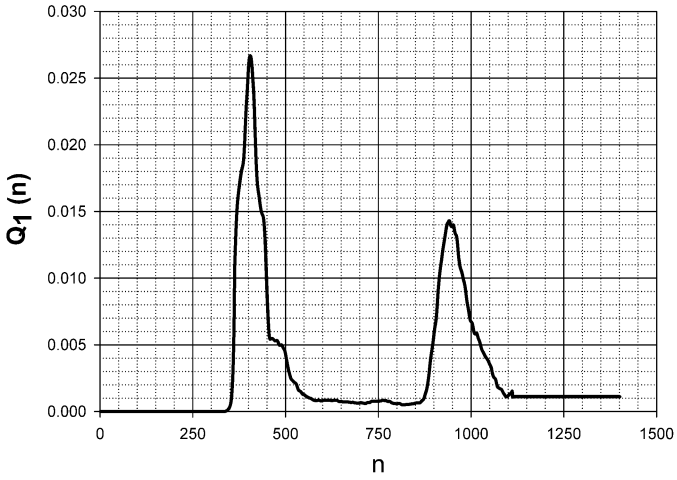

Fig. 6. Estimated $Q_1(n)$ used for the computation of $G_k(n)$ during vasodilation assessment. It contains the expected vasodilation dynamics along the sequence. Instants with higher value of $Q_1(n)$ correspond to higher uncertainty about the chose dynamic model and, consequently, where it has to be relaxed to accommodate for possibly sudden transitions.

Therefore, only the scale factor, S_y, will be used as state variable in this stage. The scaling factor has also a nonstationary behavior as its instantaneous power changes widely over time. In this situation, the prediction model is assumed to be like in the motion compensation stage where the previous state is used to predict the current state.

Owing to the standardized acquisition protocol, the vasodilation time series has a characteristic temporal evolution, which can be exploited to give an *a priori* estimation of $Q_1(n)$. The value of $Q_1(n)$ is high when vasodilation is expected and it is lowered when no variations in the artery diameter should be found (e.g., at baselines). On the other hand, the observation noise power $Q_2(n)$ is considered constant, and it is estimated from the first 60 s when vasodilation is known to be zero. $Q_2(n)$ is assumed stationary as it mainly depends on the image quality, which can be considered uniform in time for a given sequence.

The temporal evolution of $Q_1(n)$ is shown in Fig. 6. It has been estimated from the analysis of 50 vasodilation curves (from the dataset described in Section III) that were free from artifacts and obtained with the computerized method but using a fixed $G_k(n) = 0.1$ to assess the vasodilation. The plot indicates the average instantaneous power over the 50 realizations. The 60 initial frames are processed with $G_k = 0$ to calculate Q_2 in each sequence, because no vasodilation is expected during this interval and any variation here should be regarded as measurement noise.

The values of $Q_1(n)$ and Q_2 determine $G_k(n)$ using the next equation derived in Appendix I

$$G_k(n) = \frac{-Q_1(n) + \sqrt{(Q_1(n))^2 + 4 \cdot Q_1(n) \cdot Q_2}}{2 \cdot Q_2}. \quad (8)$$

IV. Results

A. Examples

Image registration between two frames searches for the transformation that puts them into correspondence. To visually illustrate the algorithm performance, four examples are shown in Fig. 7. In four sequences, the reference frame has been aligned with the frame showing maximum FMD.

B. Evaluation

Three properties of the proposed method are analyzed: accuracy (agreement with the gold-standard), reproducibility (repeatability), and robustness (degree of automation of the measurement without apparent failure). To evaluate accuracy, a number of expert manual measurements are analyzed and utilized as gold-standard measurements. As well, to get a pattern to compare our method with, accuracy and reproducibility of these manual measurements are also calculated.

We define %FMD as measurement unit for all the sequence values analyzed and represent the relative diameter of a given frame in the sequence to the mean diameter over phase B1 expressed as percentage.

Two statistical methods are used. First, we used Bland–Altman plots [23], a classical method to define limits of agreement between two measurement techniques as indicated by $d \pm 1.96 \cdot \mathrm{SD}$ where d is the mean difference (bias) and SD is the standard deviation of the differences.

Second, we used analysis of variance to estimate the variability (reproducibility) of repeated measurements on every frame. We expressed these also as coefficient of variation (CV), obtained from the mean value (m_x) and the standard deviation (SD_x) of the %FMD measurements as indicated

$$\mathrm{CV} = \frac{\mathrm{SD}_{\%\mathrm{FMD}}}{m_{\%\mathrm{FMD}}}. \quad (9)$$

1) Manual Measurements: Manual measurements of arterial diameter were performed in 117 frames corresponding to four sequences of different image quality. Three experts assessed each frame twice in independent sessions. In each sequence several frames were measured: one out of ten in phase B1 (frame number $1, 11 \ldots 61$) and one out of 50 during the rest of the test (frame number $101, 151 \ldots$). Depending on the duration of the sequence the total number of measured frames was between 28 and 30 per sequence.

Each diameter measurement was obtained by manually fitting a spline to the inner contour of each arterial wall. The diameter was defined as the average distance between both spline curves (see Appendix II). The vasodilation measurements were obtained by dividing the manually obtained diameters by the average diameter over phase B1; the dilation was finally expressed as a percentage, getting %FMD values as defined before.

Gold-standard measurements were derived from these 117 frames. The grand-average of the six diameter measurements done by the three observers is considered the gold-standard arterial diameter estimate for each frame. The gold-standard dilation measurements are obtained by dividing these estimated diameters by the grand-average diameter over phase B1 for each sequence, to get %FMD values. Accuracy, reproducibility, and intraobserver and interobserver variability of manual measurements were analyzed.

i) **Accuracy**. Fig. 8 shows the Bland–Altman plots comparing the intersession average measurement for each observer and the gold-standard measurements. The biases and SD of the differences for the three observers

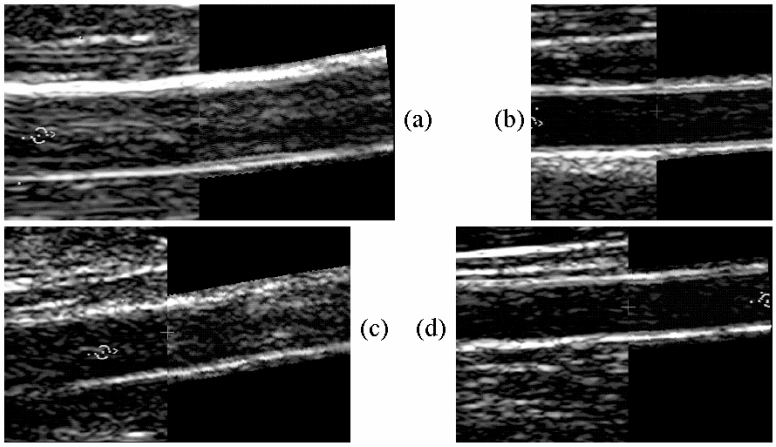

Fig. 7. Four registration examples of four sequences of different image quality. Each figure shows the FMD frame where maximum vasodilation occurs (left) registered to the reference B1 frame (right).

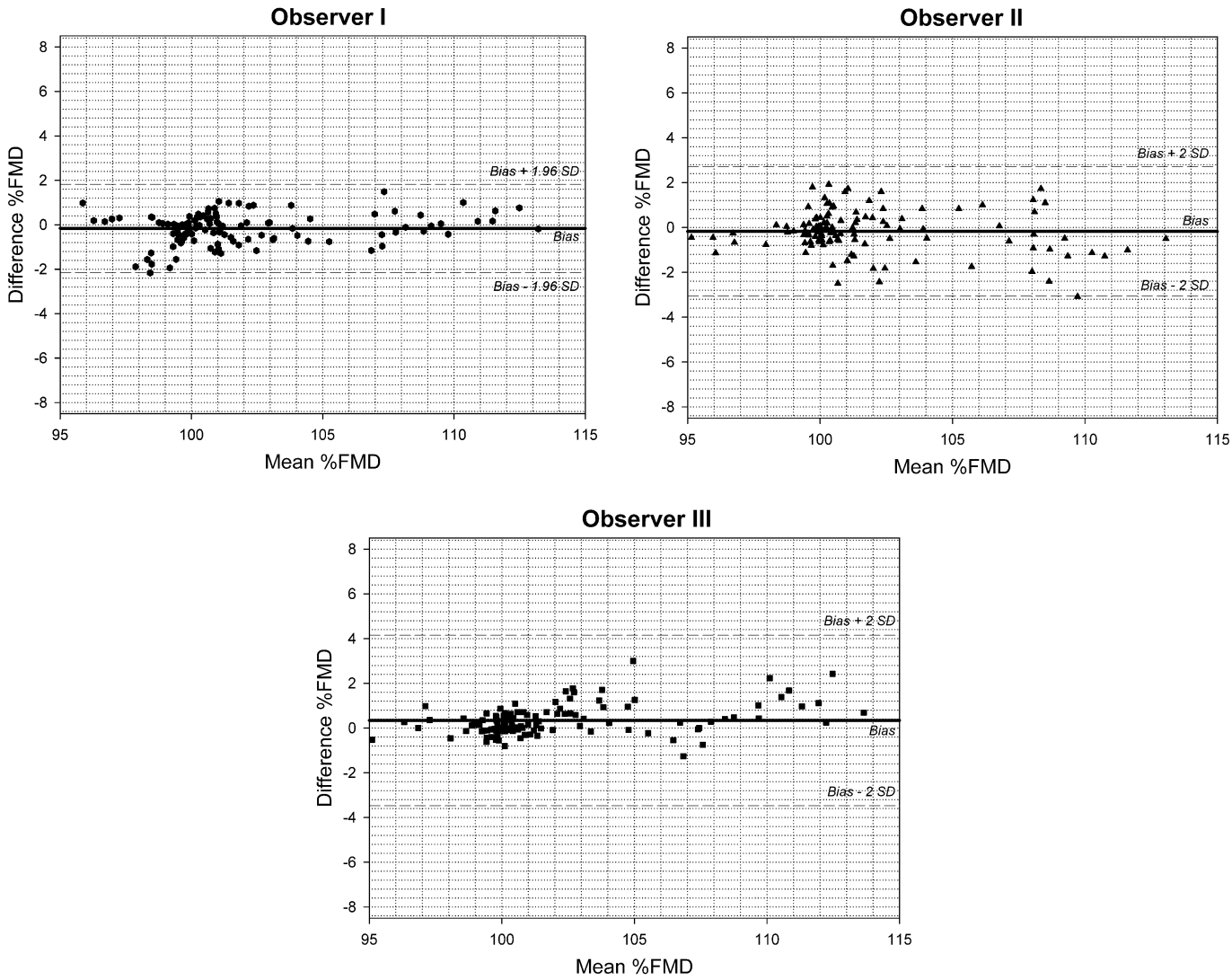

Fig. 8. Bland–Altman plots comparing the intersession measurement average versus the gold-standard measurements. The horizontal and vertical axes indicate the average %FMD and the difference %FMD, respectively.

are given in Table III. SDs are corrected to take into account repeated measurements according to the method proposed by Bland and Altman [25].

ii) **Reproducibility**. The CV of each group of six measurements is calculated for each one of the 117 manually measured frames. This CV is averaged for all the frames

TABLE III
ACCURACY OF MANUAL MEASUREMENTS. BIAS AND STANDARD DEVIATION OF THE DIFFERENCES (SD_c), CORRECTED FOR REPEATED MEASUREMENTS, BETWEEN MANUAL AND GOLD-STANDARD %FMD MEASUREMENTS. SD_m AND SD_w, STAND FOR THE SD OF THE INTERSESSION AVERAGE DIFFERENCES, AND THE WITHIN-OBSERVER VARIABILITY

	Obs I	Obs II	Obs III
Bias (%FMD)	-0.16	-0.18	0.34
SD_m (±%FMD)	0.68	0.94	0.68
SD_w (±%FMD)	0.74	1.14	1.41
SD_c (±%FMD)	0.86	1.24	1.20

TABLE IV
REPRODUCIBILITY OF MANUAL AND AUTOMATED MEASUREMENTS. MEAN AND SD OF CV (%) MEASURED WITH RESPECT TO %FMD VALUES

CV (m ± SD)	Sequence A	Sequence B	Sequence C	Sequence D	Overall
Manual (%)	0.95 ± 0.5	1.20 ± 0.4	0.71 ± 0.6	1.35 ± 0.6	1.04 ± 0.6
Computerized (%)	0.23 ± 0.1	0.26 ± 0.1	0.32 ± 0.3	0.84 ± 0.4	0.40 ± 0.3

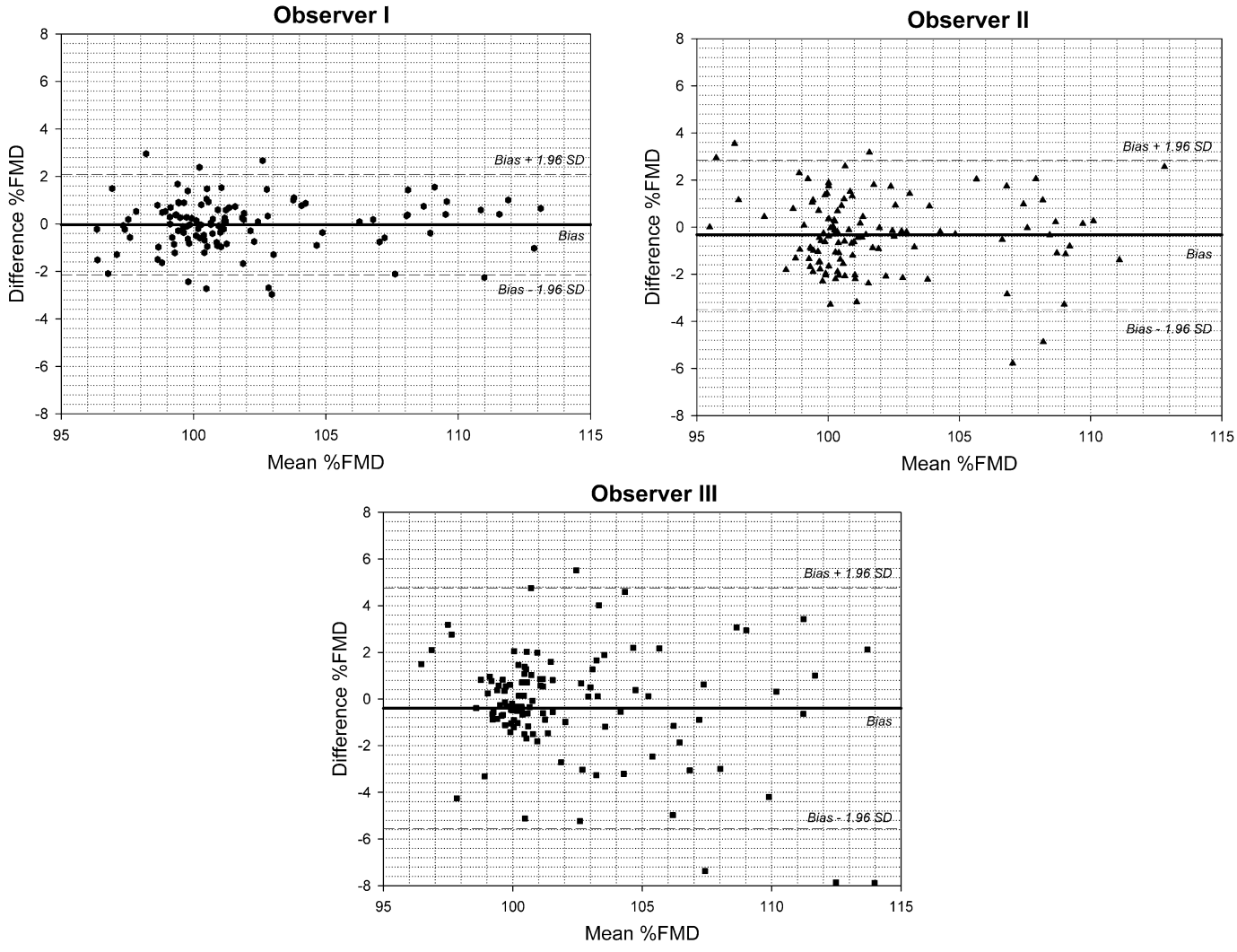

Fig. 9. Bland–Altman plots comparing the two manual sessions of dilation measurements of each observer. The horizontal and vertical axes indicate the average %FMD and the difference %FMD of the two sessions, respectively.

of each one of the four sequences, being considered the CV of the manual measurement for each sequence. These four values are averaged finally, obtaining an overall reproducibility value for manual measurements in our study. The results are shown in Table IV.

iii) **Interobserver and Intraobserver variability**. Fig. 9 shows Bland–Altman plots comparing both sessions of each observer. In order to estimate the overall interobserver and intraobserver variability of manual measurements (with correction for repeated measure-

TABLE V
TWO-WAY ANOVA OF MANUAL MEASUREMENTS OF %FMD. SSQ (SUM OF SQUARES), DOFS, MSQ (MEAN SQUARES), F (F OF SNEDECOR), P (SNEDECOR TEST SIGNIFICANCE)

Source of variation	SSq	DOF	MSq	F	p
Frame	9329.083	116	80.423	62.82	<0.0001
Observer	19.415	2	9.708	7.58	0.0006
Observer × Frame	359.752	232	1.551	1.21	0.0529
Session	449.370	351	1.280		
Total	10157.620	701			

ments) we carried out the procedure proposed by Bland and Altman in [24]. To this end, a two-way analysis of variance (ANOVA) with repeated measurements was performed using Analyze-it v 1.68 (Analyze-It Software Ltd, Leeds, U.K.). The two-way ANOVA was controlled by observer and measurement frame as fixed factors and by the session number as random factor (Table V). From this analysis, the interobserver and intraobserver within-frame %FMD SDs were 1.20% and 1.13%, respectively.

2) Computerized Measurements: The scaling factor in the direction normal to the vessel axis that relates each frame to the reference frame constitutes the vasodilation parameter output by the automatic method. As a consequence, the measurements are normalized to the arterial diameter of the reference frame. This normalization is different to that of the gold-standard dilation measurements, which, as described before, were normalized for each sequence to the grand-average diameter over phase B1. To make the computerized measurements comparable to the gold standard, a new normalization of the former measurements is necessary. To this end, the values measured at each frame are divided by the average values over all measurements of phase B1, and are multiplied by a factor 100 to obtain %FMD values.

a) Choosing a Similarity Measure: Several similarity measures traditionally used in image registration were compared in order to select the most appropriate one. Thus, the four sequences where gold-standard measurements were available were processed using the six similarity measures introduced in Table I. Finally, gold-standard vasodilations were compared with the automated vasodilations computed using each registration measure. Table VI indicates that NMI yields the most accurate estimates although the results are only marginally better than using MI. NMI is, therefore, the similarity measure selected.

b) Accuracy: Fig. 10 shows a Bland–Altman plot comparing the automated versus the gold-standard measurements. The SD of the differences is 1.05%. The dilation curves obtained by the proposed method are superimposed to the gold-standard measurements in Fig. 11 where we also include the 95% confidence interval of the gold-standard measurements for comparison.

c) Robustness: The whole set of 195 sequences were processed with the proposed method (more than 280 000 frames). The overall result was ranked according to the ability to recover the clinically relevant information from the corresponding vasodilation curve. The results were classified as good, useful and bad, depending on the amount and severity of the artifacts present in the curve. When, in the opinion of an expert sonographer, there were no evident artifacts in the vasodilation curve, the result was scored as good (77.3% of sequences). Artifacts considered were, for instance, lack of convergence or unusual vasodilation evolution. A vasodilation curve was ranked as useful (5.2% of sequences) when artifacts appear only in the DI phase(Fig. 2), where no medical information is to be extracted, and therefore, it would still be possible to get clinical information from the other phases.

TABLE VI
COMPARISON BETWEEN DIFFERENT SIMILARITY METRICS. BIAS AND DIFFERENCE SD IN THE COMPARISON BETWEEN THE GOLD STANDARD MEASURES AND THE AUTOMATIC DILATION OBTAINED WITH DIFFERENT SIMILARITY MEASURES. FIGURES ARE REPORTED CORRESPOND TO %FMD VALUES

	NMI	MI	GCC	JE	CC	SSD
Bias (%FMD)	+0.05	+0.11	+0.25	-1.00	+1.03	+1.68
SD (± %FMD)	1.05	1.08	2.02	2.49	2.55	3.92

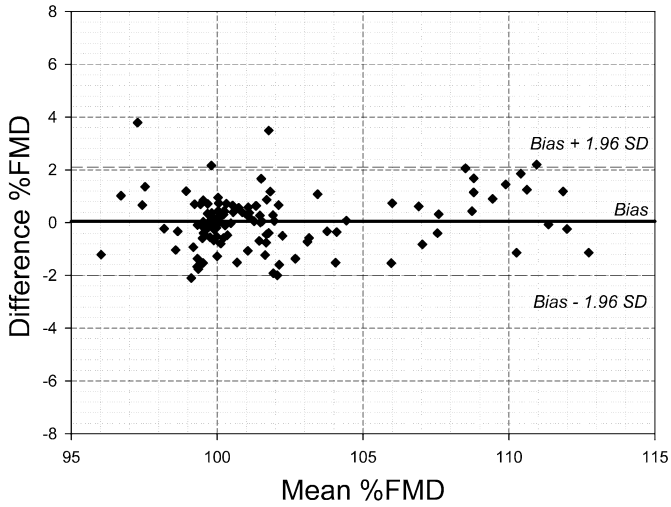

Fig. 10. Bland–Altman plot comparing the automatic measurements (using NMI as similarity measure) versus the gold standard. The horizontal and vertical axes indicate the average %FMD and the difference %FMD of the automatic measurements and the gold-standard measurements, respectively.

d) Reproducibility: The four sequences with gold-standard measurements were analyzed with the automatic method in six independent runs. Each time a different reference frame was randomly chosen from within phase B1 and it was manually preprocessed (horizontal repositioning of the vessel and removal of extra luminal structures). The CV was computed using as a basis the six dilation measurements for each frame of each sequence. Subsequently, the mean CV in each sequence was obtained by averaging the CV values of the frames where manual

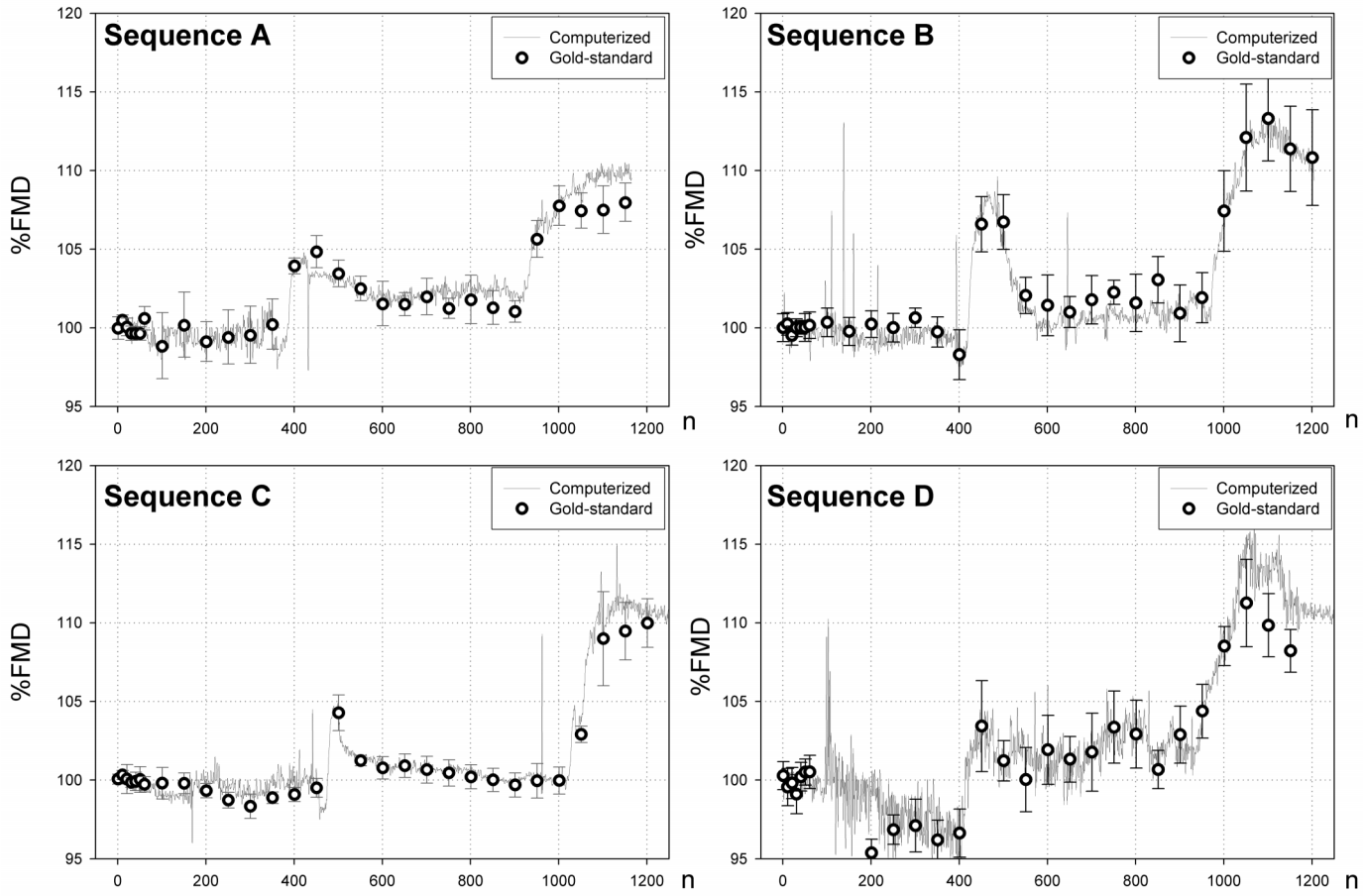

Fig. 11. FMD curves obtained by the proposed automated method (—), and by the gold-standard measurements (◯). Error bars show the 95% confidence interval of the gold-standard measurements for comparison.

measurements were also carried out. These four values are presented in Table IV.

V. Discussion

Artery vasodilation assessment is a complex task owing to the poor quality of US image sequences and the small range of the vasodilation that has to be measured. Previous attempts to solve this problem were based on detecting the edges of the arterial wall. These methods have been successful to some extent; however, edge detection in ultrasound is prone to fail due to the presence of speckle noise, poor-quality edge definition, and acoustic shadows. In our opinion, these techniques are based on low-level features with a poor reliability.

Our method, on the contrary, deals with the images in a more global manner. We model vasodilation as a scaling factor between frames that can be recovered by means of image registration techniques. The effect of low-level artifacts is, therefore, minimized as the registration measure is computed using all the information present in the whole image, and not just at the edges.

Results obtained with the automated method were better than those measured manually by medical experts. The proposed method presents a negligible bias (0.05%FMD) whereas the bias of the manual measurements depends on the observer (range -0.16 to $+0.34\%\mathrm{FMD}$). The SD of the differences between the automated and the gold-standard measurements is 1.05%FMD, which is slightly lower than the intraobserver and interobserver variabilities of manual measurements (1.13%FMD and 1.20%FMD, respectively). From the dilation CV, the proposed method has also shown to present better reproducibility ($\mathrm{CV} = 0.40\%$) than the manual procedure ($\mathrm{CV} = 1.04\%$).

The method is reasonably fast. Our experiments were carried out on a PC (Pentium III at 600 MHz) under RedHat 7.2 Linux operating system. The registration algorithm and the Kalman filtering are both coded in C++ without a thorough code optimization since the implementation of the registration method is a general-purpose software not specifically devised for this application. Under these constraints, the mean execution times per frame are 6.4 s ($\mathrm{SD} = 0.8$ s) and 4.0 s ($\mathrm{SD} = 1.2$ s) for the first and second phase, respectively. This time also incorporates outputting of progress information. From our experience with the software, we think that these figures could still be cut down substantially by customizing and further optimizing several parts of the code.

The vasodilation model used in this approach has also some potential limitations. Here, dilation is recovered by means of reduced similarity transformation between each frame and the reference one. However, this implicitly assumes that the wall thickness dilates in the same way that the artery does, while it may remain constant or even thin during lumen dilation. The unstable

presence of the lumen-intimae boundary could potentially affect the registration results. Finally, structures stuck to the outer part of the arterial wall may introduce errors in the vasodilation measurements since they make it more difficult to adequately pad the reference frame. The results obtained in this paper seem to indicate, however, that the vasodilation model outlined in this work is a reasonable simplification.

Motion compensation is necessary to avoid potential sources of bias in the subsequent estimation of vasodilation and to ensure that vasodilation is measured by comparing the same artery segment in two different frames. Nevertheless, stable motion references are required to succeed in motion recovery and avoiding indetermination of the correct alignment in the longitudinal direction of the artery. Moreover, only 2-D information is available in the image to correct a problem that is intrinsically 3-D in nature.

Another advantage of motion compensation is that it makes unnecessary the manual [12], [13] or automatic [15] tracking of a region of interest (ROI) in the image sequence. This ROI tracking is required for the edge detection of some of the methods proposed in the literature. Our technique requires a simple preprocessing of only the reference frame. The interaction required is minimal (only rough delineation of two lines) and introduces a small variability (it is included in the CV of 0.40% obtained in the reproducibility study).

The initialization of the registration algorithm is a very important aspect. This initial transformation should fall inside the capture range of the algorithm [21] whose size depends on many factors, and its determination is not possible *a priori*. Some of these factors are the image quality, the line thickness of the arterial walls and the preprocessing made to the images. It is common that some frames appear with poor image quality along the sequence due to patient's motion. One of these frames may probably lead to erroneous registration values. To reduce error propagation Kalman filtering has shown to be very valuable.

Finally, it is important to recall that the proposed tracking strategy depends on a model of mean arterial vasodilation. This model was estimated from a number of training vasodilation curves, which corresponded to young healthy volunteers. Therefore, this model could bias the analysis of sequences coming from a general population or in specific subject groups like old obese patients. This limitation could be overcome by using a larger training set for building the mean vasodilation model or by having several models for different age groups.

VI. Conclusion

A new method to assess brachial artery vasodilation in US sequences has been presented. This method, based on image registration, minimizes the effect of low-level artifacts. It also incorporates a motion compensation phase, which relieves the operator of manually tracking a ROI.

The method is accurate ($\mathrm{bias} = +0.05\%$, and limits of agreement $\pm 2.05\%\mathrm{FMD}$), has better reproducibility ($\mathrm{CV} = 0.40\%$) than manual measurements ($\mathrm{CV} = 1.04\%$), and is robust, yielding clinically relevant information in at least 80% of the sequences in an uncontrolled clinical setting. Finally, the method requires minimal user intervention having limited effect on the reproducibility of the measurements.

Appendix I
Calculation of $G_k(n)$

In the Kalman filter, the Kalman Gain (G_k) weights the innovation contributed by each new input data. The necessary elements for its calculation are: as follows.

- **State model**: transition matrix $\mathbf{F}(n, n-1)$ and noise process power $\mathbf{Q_1}(n)$. The matrix $\mathbf{F}(n, n-1)$ models the dynamics of the state and $\mathbf{Q_1}(n)$ models the uncertainty of the dynamic model.
- **Observation model**: observation matrix $\mathbf{C}(n)$ and noise process power $\mathbf{Q_2}(n)$. The matrix $\mathbf{C}(n)$ relates the (hidden) state and the observable/measurable variables while $\mathbf{Q_2}(n)$ models the measurement error.
- **Measurements**: $\mathbf{Y}(n)$.

The transition matrix is used to predict the next state from the last state estimate

$$\hat{\mathbf{X}}(n) = \mathbf{F}(n, n-1) \cdot \tilde{\mathbf{X}}(n-1). \tag{10}$$

The next observation, $\hat{\mathbf{Y}}(n)$, is predicted using the observation matrix, $\mathbf{C}(n)$, and the state prediction

$$\hat{\mathbf{Y}}(n) = \mathbf{C}(n) \cdot \hat{\mathbf{X}}(n). \tag{11}$$

The difference between the observation $\mathbf{Y}(n)$ and the data prediction is the innovation $\boldsymbol{\alpha}(n)$

$$\boldsymbol{\alpha}(n) = \mathbf{Y}(n) - \hat{\mathbf{Y}}(n). \tag{12}$$

The state estimate is computed by adding the state prediction to the innovation weighted by the Kalman Gain

$$\tilde{\mathbf{X}}(n) = \hat{\mathbf{X}}(n) + \mathbf{G}_K(n) \cdot \boldsymbol{\alpha}(n). \tag{13}$$

Several new matrices are calculated to determine $\mathbf{G}_K(n)$: the correlation matrix of the *a priori* state-error ($\mathbf{E}(n|n-1)$), the correlation matrix of the *a posteriori* state-error ($\mathbf{E}(n|n)$) and the correlation matrix of the innovation process $\mathbf{E}(n)$. Four equations are needed

$$\begin{aligned}
\mathbf{E}(n|n-1) =& \mathbf{F}(n, n-1) \cdot \mathbf{E}(n-1|n-1) \\
& \cdot \mathbf{F}^H(n, n-1) + \mathbf{Q}_1(n) && (14)\\
\mathbf{E}(n) =& \mathbf{C}(n) \cdot \mathbf{E}(n|n-1) \cdot \mathbf{C}^H(n) + \mathbf{Q}_2(n) && (15)\\
\mathbf{G}_K(n) =& \mathbf{E}(n|n-1) \cdot \mathbf{C}(n) \cdot \mathbf{E}^{-1}(n) && (16)\\
\mathbf{E}(n|n) =& [1 - \mathbf{G}_K(n) \cdot \mathbf{C}(n)] \cdot \mathbf{E}(n|n-1). && (17)
\end{aligned}$$

In our case, the state vector is made up of the artery position, orientation, and the vasodilation factor; $\mathbf{C}(n)$ is the identity, as the observation variables are simply a noisy version of the state variables. Moreover, all matrix expressions become scalar, since the state prediction model is zero-order. Under these assumptions, and the hypothesis that the covariance of the *a priori* state-error equals the covariance of the *a posteriori* state error (what would happen in a stationary situation), the last four equations boil down to

$$G_K^2(n) \cdot Q_2(n) + G_K(n) \cdot Q_1(n) - Q_1(n) = 0. \tag{18}$$

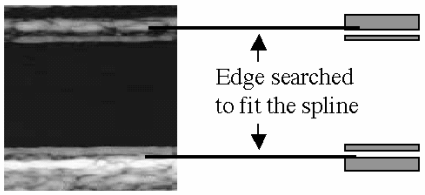

Fig. 12. Manual fitting of a spline to the arterial wall.

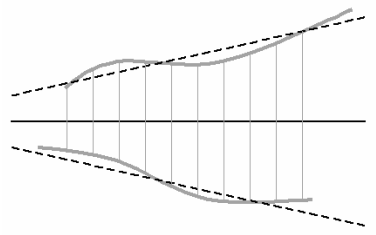

Fig. 13. Average diameter estimation. The diameter is the mean length of the segments (thin continuous gray lines) perpendicular to the bisector (continuous black line) between the regression lines (dashed black lines) of both splines. Nonparallelism and tortuosity of the splines representing the arterial walls have been exaggerated to clarify the example.

The approximation made in this expression of $G_K(n)$ is only introduced at points when there is a sudden change in $Q_1(n)$ or $Q_2(n)$. At these points, the exact calculation shows certain inertia when dealing with the transitions. These errors are negligible because the estimates of the functions $Q_1(n)$ and $Q_2(n)$ that we have chosen have already soft transitions ($Q_1(n)$) or are constant ($Q_2(n)$).

Appendix II
Distance Between Two Splines

Each manual measurement requires fitting of a cubic spline to the edge of each arterial wall. The distance between both splines is the arterial diameter. The line is placed at the inner edge of the media as showed in Fig. 12.

The distance is calculated as follows (see Fig. 13).

Step 1) The orientation of each spline is calculated by means of a linear regression.

Step 2) The mean orientation of both splines is calculated using the bisector of the two calculated regression lines.

Step 3) Perpendicular lines to this bisector are traced, every ten pixels, finding the intersection points with the two splines.

Step 4) The average distance between all pairs of points found is the arterial diameter.

Acknowledgment

The authors would like to express their gratitude to Dr. D. Rueckert for providing them with his implementation of Studholme's algorithm. They wish to thank M.L. Gimeno, MD, and A.G. Frangi, MD for providing manual measurements for the evaluation study, and Dr. S. Olmos for useful suggestions to improve the manuscript. Finally, the authors acknowledge that the AGEMZA Project is supported by the Spanish Ministry of Health and Consumption under Grant FIS 99/0600. The clinical research was supported in part by the Diputación General de Aragón under Grant P58/98.

References

[1] M. C. Corretti, T. J. Anderson, E. J. Benjamin, D. Celermajer, F. Charbonneau, M. A. Creager, J. Deanfield, H. Drexler, M. Gerhard-Herman, D. Herrington, P. Vallance, J. Vita, and R. Vogel, "International brachial artery reactivity task force'Guidelines for the ultrasound assessment of endothelial-dependent flow-mediated vasodilation of the brachial artery'," *Amer. J. Cardiol.*, vol. 39, no. 2, pp. 257–265, 2002.

[2] H. Teregawa, M. Kato, J. Kurokawa, T. Yakagata, H. Matsuura, and K. Chayama, "Usefulness of flow-mediated dilation of the brachial artery and/or the intima-media thickness of the carotid artery in predicting coronary narrowing in patients suspected of having coronary artery disease," *Amer. J. Cardiol.*, vol. 88, pp. 1147–1151, 2001.

[3] J. P. Cooke, E. Rossitch Jr, N. A. Andon, J. Loscalzo, and V. J. Dzau, "Flow activates an endothelial potassium channel to release an endogenous nitrovasodilator," *J. Clin. Investigat.*, vol. 88, no. 5, pp. 1663–1671, 1991.

[4] L. I. Sinoway, C. Hendrickson, W. R. Davidson Jr, S. Prophet, and R. Zelis, "Characteristics of flow-mediated brachial artery vasodilation in human subjects," *Circ. Res.*, vol. 64, no. 1, pp. 32–42, 1989.

[5] D. S. Celermajer, K. E. Sorensen, V. M. Gooch, D. J. Spiegelhalter, O. I. Miller, I. D. Sullivan, J. K. Lloyd, and J. E. Deanfield, "Non-invasive detection of endothelial dysfunction in children and adults at risk of atherosclerosis," *Lancet*, vol. 340, no. 8828, pp. 1111–1115, 1992.

[6] K. L. Hardie, S. Kinlay, D. B. Hardy, J. Wlodarczyk, J. S. Silberberg, and P. J. Fletcher, "Reproducibility of brachial ultrasonography and flow-mediated dilatation (FMD) for assessing endothelial function," *Aust. N. Z. J. Med.*, vol. 27, no. 6, pp. 649–652, 1997.

[7] P. J. Touboul, P. Prati, P. Q.-Y. Scarabin, V. Adrai, E. Thibout, and P. P. Ducimetire, "Use of monitoring software to improve the measurement of carotid wall thickness by B-mode imaging," *J. Hypertension*, vol. 10, no. Suppl. 5, pp. S37–S41, 1992.

[8] J. Gariepy, M. Massonneau, J. Lavenson, D. Haudes, and A. Simon, "Evidence for *in vivo* carotid and femoral wall thickness in human hypertension," *Hypertension*, vol. 22, no. 1, pp. 111–118, 1993.

[9] R. H. Selzer, H. N. Hodis, H. Kwong-Fu, W. J. Mack, P. L. Lee, C. R. Liu, and C. H. Liu, "Evaluation of computerized edge tracking for quantifying intima-media thickness of the common carotid artery from B-mode ultrasound images," *Atherosclerosis*, vol. 11, pp. 1–11, 1994.

[10] R. J. Kozick, "Detecting interfaces on ultrasound images of the carotid artery by dynamic programming," *Proc. SPIE*, vol. 2666, pp. 233–241, 1996.

[11] T. Guvstavsson, Q. Liang, I. Wendelhag, and J. Wikstrand, "A dynamic programming procedure for automated ultrasonic measurement of the carotid artery," in *Proc. IEEE Computers Cardiology 1994*, pp. 297–300.

[12] M. Sonka, W. Liang, and R. M. Lauer, "Flow-mediated dilation in brachial arteries: Computer analysis of ultrasound image sequences," *CVD Prevention*, vol. 1, no. 2, pp. 147–155, 1998.

[13] Q. Liang, I. Wendelhag, J. Wikstrand, and T. Gustavsson, "A multiscale dynamic programming procedure for boundary detection in ultrasonic artery images," *IEEE Trans. Med. Imag.*, vol. 19, Feb. 2000.

[14] M. Preik, T. Lauer, C. Heiss, S. Tabery, B. E. Strauer, and M. Kelm, "Automated ultrasonic measurement of human arteries for the determination of endothelial function," *Ultraschall. Med.*, vol. 21, no. 5, pp. 195–8, 2000.

[15] L. Fan, P. Santago, H. Jiang, and D. M. Herrington, "Ultrasound measurement of brachial flow-mediated vasodilator response," *IEEE Trans. Med. Imag.*, vol. 19, pp. 621–631, June 2000.

[16] L. Fan, P. Santago, W. Riley, and D. M. Herrington, "An adaptive template-matching method and its application to the boundary detection of brachial artery ultrasound scans," *Ultrasound Med. Biol.*, vol. 27, no. 3, pp. 399–408, 2001.

[17] M. Mignotte and J. Meunier, "A multiscale optimization approach for the dynamic contour-based boundary detection issue," *Comput. Med. Imag. Graph.*, vol. 25, pp. 265–275, 2001.

[18] R. J. Woodman, D. A. Playford, G. F. Watts, C. Cheetham, C. Reed, R. R. Taylor, I. B. Puddey, L. J. Beilin, V. Burke, T. A. Mori, and D. Green, "Improved analysis of brachial artery ultrasound using a novel edge-detection software system," *J. Appl. Physiol.*, vol. 91, no. 2, pp. 929–37, 2001.

[19] V. R. Newey and D. K. Nassiri, "Online artery diameter measurement in ultrasound images using artificial neural networks," *Ultrasound Med. Biol.*, vol. 28, no. 2, pp. 209–16, 2002.

[20] C. Studholme, D. L. G. Hill, and D. J. Hawkes, "An overlap invariant entropy measure of 3D medical image alignment," *Pattern Recogn.*, vol. 32, pp. 71–86, 1999.
[21] ——, "Automated three-dimensional registration of magnetic resonance and positron emission tomography brain images by multiresolution optimization of voxel similarity measures," *Med. Phys.*, vol. 24, no. 1, 1997.
[22] R. E. Kalman, "A new approach to linear filtering and prediction problems," *Trans. ASME-J. Basic Eng.*, ser. D, vol. 82, pp. 35–45, 1960.
[23] D. G. Altman, *Practical Statistical Research*. London, U.K.: Chapman & Hall, 1991.
[24] J. M. Bland and D. G. Altman, "Statistical methods for assessing agreement between two methods of clinical measurement," *Lancet*, vol. 1, no. 8476, pp. 307–10, Feb 1986.
[25] ——, "Measuring agreement in method comparison studies," in *Statist. Meth. Med. Res.*, J. M. Bland and D. G. Altman, Eds., 1999, vol. 8, pp. 135–60.